# A study on the Structure, vibrational spectral assignments, UV, NMR, MESP and NLO properties of 2-(hydroxymethyl)-5- methyl phenol Molecule

D. Jaya Reshmi[1], D. Arul Dhas[*2]

[1]Research Scholar, Register Number: 11975, Department of Physics & Research Centre, Nesamony Memorial Christian College Marthandam – 629165. Affiliated to Manonmaniam Sundaranar University, Abishekapatti, Tirunelveli – 627012, Tamil Nadu, India.

[2]Associate Professor, Department of Physics & Research Centre, Nesamony Memorial Christian College Marthandam – 629165. Affiliated to Manonmaniam Sundaranar University, Abishekapatti, Tirunelveli – 627012, Tamil Nadu, India.

***Abstract:*** Vibrational features, optical and electronic properties of organic compound 2-(hydroxymethyl)-5- methyl phenol (HMP) molecule have been studied. Spectral and electronic properties were studied by FT-IR, FT-Raman and UV-visible spectroscopic technique with Moller Plesset (MP2) method. The intramolecular charge transfer interactions leading to nonlinear optical response have been analysed by natural bond orbital analysis. The first and second order hyperpolarizabilities were calculated at MP2 level using 6-31G (d) hybrid functional. The optimized geometric parameters (bond lengths and bond angles) were compared with experimental value. The stability of the molecule arising from hyperconjugative interactions and the charge delocalization has been analysed using natural bond orbital (NBO) analysis. The calculated HOMO and LUMO energies shows that charge transfer occur within the molecule. Furthermore, molecular electrostatic potential maps (MESP) of the molecule have been calculated.

***Keywords***: NBO, MESP, NLO, MP2, PES

## 1. INTRODUCTION

Nonlinear optical effects depend on the change in polarizability of the electrons in the π bonding orbitals. The organic molecules exhibiting second-order non linear optical (NLO) properties has also been motivated by the irtremendous potential for application in optical communications, optical computing, data storage, dynamic holography, harmonic generators, frequency mixing and optical switching [1]. The carbon atom in the organic dyes can form a variety of stable bonds due to its delocalized electronic charge distributions. Addition of suitable acceptors or donors into the π-conjugated system increases asymmetric electronic distribution which leads to an increase in higher order optical nonlinearities. The organic HMP molecule used in the industry to dye wool and silk, cosmetics for external use and it is a derivative. The main functional groups present in HMP molecule are methyl group, hydroxyl group and hydroxyl methyl group. The delocalization behaviour of π electrons and donor acceptor interactions of organic dyes leads the nonlinear nature. The molecular formula for HMP molecule is $C_8H_{10}O_2$. The molecular weight of HMP molecule is 138.166g/mol. The present work, aim to report the results of the optimized geometry, vibrational frequencies, NBO analysis, HOMO–LUMO analysis, atomic charges, molecular hyperpolarizability and potential energy surface scan study of HMP molecule by using the MP2/6-31G(d) level. The redistribution of electron density (ED) in various bonding and antibonding orbitals and $E^{(2)}$ energies has been calculated by natural bond orbital (NBO) analysis by MP2 method to give clear evidence of stabilization originating from the hyperconjugation of various intramolecular interactions.

Molecular electrostatic potential (MESP) contour map shows the various electrophilic region of the HMP molecule.

## 2. Experimental details

The compound was purchased from sigma-Aldrich with 99%purity and used without further purification. The FT-IR spectrum of the HMP molecule was traced in the region of 4000 to 400 $cm^{-1}$ using Perkin-Elmer Spectrometer with a resolution of 1 $cm^{-1}$. FT-Raman spectrum in the range of 3500-50 $cm^{-1}$ was obtained from Bruker RFS 27: standalone FT- Raman spectrometer with resolution 2 $cm^{-1}$. The UV-visible absorption spectrum was recorded on Perkin Elmer Lambda-35 spectrophotometer in the range of 700-200 nm at a resolution of 1 nm. The $^{1}H$ and $^{13}C$ NMR spectra were recorded (in CDCl3) on Bruker AVANE III 500 MHz (AV500) NMR spectrometer at 300 MHz for $^{1}H$ and 75 MHz for $^{13}C$ NMR using tetramethylsilane (TMS) as an internal standard.

## 3. Computational details

All quantum chemical computational work have been performed using Gaussian '09W programme package [2] and the ground-state equilibrium geometries were optimized at Møller Plesset (MP2) perturbation theory at the level using correlation hybrid functional with 6-31G (d) basis set. Visualization and checking of calculated data were done by using the CHEMCRAFT program [3] and Gauss View program [4]. The vibrational modes were assigned on the basis of potential energy distribution analysis (PED) using VEDA 4 program [5]. Natural bond orbital (NBO) and natural population analysis (NPA) were performed using NBO 3.1 program [6]. Excitation energies, absorption wavelengths and oscillator strengths associated with some electronic transitions have been carried out by PCM-TD-DFT method at the same level of basis set [7] in acetone, DMSO and ethanol environment. The polarizability (α), hyperpolarizability (β) and the electric dipole moment were calculated by MP2/6-31G (d) method. These parameters specify the NLO characteristics along with molecular orbitals.

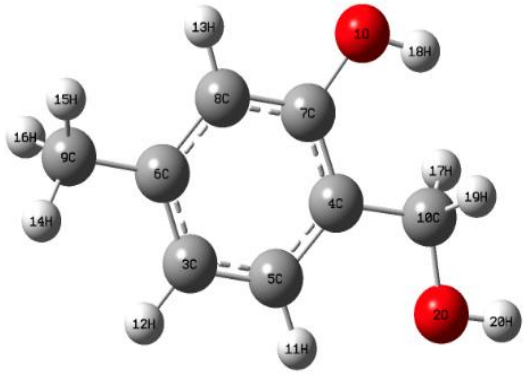


Fig.1: Optimised molecular structure of HMP molecule.

**Table 1: Selected bond lengths and bond angles of HMP molecule by MP2/6-31G (d) in comparison with the XRD data**

| Optimized bond length ( Å ) | | | Optimized bond angle (°) | | |
|---|---|---|---|---|---|
| **Parameter** | **Expt ( Å )** | **Calc ( Å )** | **Parameter** | **Expt (°)** | **Calc (°)** |
| $O_1$-$C_7$ | 1.349 | 1.381 | $C_3$-$C_5$-$C_4$ | 121.9 | 120.8 |
| $C_3$-$C_5$ | 1.385 | 1.393 | $C_5$-$C_3$-$C_6$ | 117.2 | 120.8 |
| $C_3$-$C_6$ | 1.383 | 1.400 | $C_5$-$C_4$-$C_7$ | 119.5 | 118.2 |
| $C_4$-$C_5$ | 1.402 | 1.397 | $C_3$-$C_6$-$C_8$ | 123.2 | 118.4 |
| $C_4$-$C_7$ | 1.390 | 1.402 | $C_6$-$C_3$-$C_9$ | 121.5 | 121.0 |
| $C_4$-$C_{10}$ | 1.471 | 1.507 | $O_1$-$C_7$-$C_4$ | 119.5 | 122.9 |
| $C_6$-$C_8$ | 1.390 | 1.396 | $O_1$-$C_7$-$C_8$ | 120.7 | 116.0 |
| $C_7$-$C_8$ | 1.412 | 1.394 | $C_4$-$C_7$-$C_8$ | 119.7 | 120.9 |
| $C_{10}$-$H_{17}$ | 0.929 | 1.103 | $C_5$-$C_4$-$C_{10}$ | 119.1 | 121.8 |
| $O_1$-$H_{18}$ | 0.820 | 0.971 | $C_7$-$C_4$-$C_{10}$ | 121.3 | 119.9 |
| | | | $C_6$-$C_8$-$C_7$ | 118.2 | 120.6 |
| | | | $C_6$-$C_8$-$H_{13}$ | 119.9 | 121.2 |
| | | | $C_7$-$C_8$-$H_{13}$ | 121.7 | 118.1 |
| | | | $C_7$-$O_1$-$H_{18}$ | 109.4 | 109.6 |

## 4. RESULTS AND DISCUSSION

### **4.1.** Optimized geometries

The optimized molecular geometry of the HMP molecule is calculated using Gaussion'09W program. The complete optimized geometrical parameters are given in Table 1. The geometry optimization of the compound was carried out using MP2/6-31G (d) basis set. Fig.1 depicts the optimized molecular structure of the compound. The calculated values by MP2 method was compared with x-ray diffraction results [8]. The C-C aromatic bond distances fall in the range from 1.412 to 1.540 Å. The bond length of $C_4$-$C_5$ is 1.397 Å. Due to the presence of hydroxy methyl group, the bond length of $C_4$-$C_7$ is 1.402Å. The bond length of $C_3$-$C_6$ is 1.400Å because of the methyl group linked with $C_3$ atom. The bond $C_6$-$C_8$ is 1.396 Å due to methyl substitution present in place hydrogen atom. The bond $C_7$-$C_8$ is 1.394 Å may be the attachment of hydroxyl group at $C_7$ atom. In methyl group, the C-H bond length values are longer and ring C-H bond length values are smaller. The bond length of $C_7$-$O_1$ is 1.381 Å and the bond length of $C_{10}$-$O_2$ is 1.230 Å. These distortions are explained in terms of the change in hybridization due to the substituent at the carbon to which it is attached.

The exocyclic bond angles $C_6$-$C_3$-$C_9$, $C_7$-$C_4$-$C_{10}$ and $C_6$-$C_8$-$C_9$ values are 121º. The $C_3$-$C_6$-$C_8$, $C_7$-$C_4$-$C_5$, $C_4$-$C_5$-$C_3$ and $C_5$-$C_3$-$C_6$ values are slightly deviated from the standard value 120º which the substitution of methyl group, hydroxyl group and the hydroxy methyl group in place of hydrogen atoms. The endocyclic bond angles$C_3$-$C_6$-$C_9$, $C_6$-$C_8$-$C_7$, $C_7$-$C_4$-$C_{10}$ are 121º.

The torsion angles $C_5$-$C_3$-$C_6$-$C_8$, $C_5$-$C_4$-$C_7$-$C_8$ and $O_1$-$C_7$-$C_4$-$C_{10}$ indicate that these groups substituted in the ortho position of phenyl ring are co-planar and in the plane of the phenyl ring. This predicts maximum conjugation of molecule with donor and acceptor groups. The difference between the experimental and

the theoretical values may be due to the weak intramolecular hydrogen bonding between the hydroxyl and the hydroxy methyl groups.

**4.2.** Vibrational Analysis

The HMP molecule consists of 20 atoms and so they have 54 normal vibrational modes. The calculated harmonic wavenumbers are usually higher than the corresponding experimental quantities because of the combination of electron correlation effects and basis set deficiencies. The vibrational frequencies of the optimized molecular structure were computed using MP2/6-31G (d) level and compared with the experimental data. Fig. 2 shows the experimental FT-IR spectra of the HMP molecule. The spectral assignments were presented in Table 2.

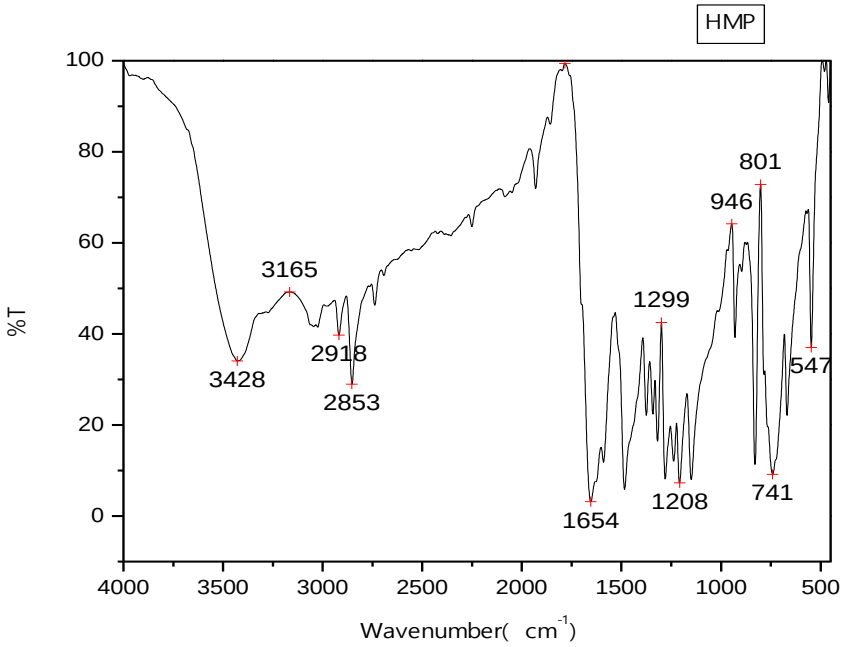


Fig. 2: Experimental FT-IR spectrum of HMP molecule.

**4.2.1** Hydroxyl (OH) Vibrations

The O-H group gives rise to three vibrations such as stretching, in plane bending and out-of-plane bending vibrations. The hydroxyl stretching vibrations are generally [9, 10] observed in the region around 3500 $cm^{-1}$. In the present case, the theoretical calculation of HMP molecule predict the anharmonic wavenumber at 3428 by MP2 method which is assigned to O-H stretching vibration, this wavenumber show negative deviation, this may be due to the presence of hydrogen bonding between hydroxymethyl ($CH_2$-OH) and hydroxyl groups. The stretching vibrational wavenumber of O-H is practically unchanged, while that of the bound O-H is red shifted. The red shift of the O-H stretching wavenumber is due to the formation of strong O-H…O hydrogen bonds by hyperconjucation between hydroxy methyl group oxygen lone electron pairs and σ*O-H antibonding orbitals. This is due to the increase in electron density occurring at σ*C=O and the antibonding orbitals σ*O-H. Consequently, these bonds become weaker and are elongated, and the respective stretching vibrational wavenumbers are red shifted [11]. The in-plane bending vibration of O-H occurs in the region 1000–1650 $cm^{-1}$ and is expected to increase in its

wavenumber and is known as couple with other vibrations. The out-of-plane mode is observed in the calculated spectrum at 404 $cm^{-1}$. The MP2 frequencies are in good agreement with both the in-plane and out-of-plane modes.

**Table : 2 Vibrational assignment of HMP molecule.**

| Wave number($cm^{-1}$) | | | IR Intensity | Raman intensity | Assignments With PED (%) |
|---|---|---|---|---|---|
| Experimental values ($cm^{-1}$) | | Calculated values ($cm^{-1}$) | | | |
| FT-IR | FT-Raman | | | | |
| 3428s | | 3566 | 3 | 5 | $^{\nu}O_1H_{18}$(95) |
| 3165m | 3074 | 3081 | 0 | 1 | $^{\nu}O_2H_{20}$(65) |
| 3041 | 3042 | 3048 | 12 | 9 | $^{\nu}C_3H_{12}$(88) |
| 3019 | 3025s | 3015 | 9 | 6 | $+^{\nu}C_5H_{11}$(10) |
| 2978 | - | 2999 | 4 | 8 | $^{\nu}C_8H_{13}$(86)Sym |
| 2918s | 2921 | 2925 | 17 | 10 | $^{\nu}$ $C_8H_{13}$(43)Asym |
| 2853vs | 2858 | 2841 | 12 | 17 | $^{\nu}C_9H_{14}$(92) |
| 1654s | 1644vs | 1630 | 27 | 58 | $^{\nu}C_9H_{14}$(79)+$^{\nu}C_9H_{15}$(92)+$^{\nu}C_9H_{16}$(63) Asym |
| 1625 | 1623 | 1613 | 13 | 100 | $^{\nu}C_9H_{14}$(79)+$^{\nu}C_9H_{15}$(92)+$^{\nu}C_9H_{16}$(63) Sym |
| 1590 | 1580 | 1564 | 41 | 42 | $^{\nu}C_9H_{14}$(11)+$^{\nu}C_9H_{15}$(18) |
| 1481w | 1479 | 1483 | 26 | 4 | $^{\nu}C_{10}H_{17}$(19) |
| - | 1454 | 1459 | 32 | 38 | $^{\nu}C_1C_6$(57) + $^{\beta}H_9C_1C_2$(12) |
| - | 1437w | 1435 | 29 | 34 | $C_{10}O_2$(99) |
| 1374 | 1378 | 1381 | 3 | 6 | $^{\nu}C_3C_5$(47)+$^{\nu}C_4C_5$(51) +$^{\nu}C_6C_8$(57) |
| 1341 | 1344 | 1326 | 36 | 31 | $^{\nu}C_3C_5$(43)+$^{\nu}C_4C_5$(52) +$^{\nu}C_6C_8$(37) |
| 1319vw | 1314m | 1317 | 4 | 42 | $^{\nu}C_3C_5$(71)+$^{\nu}C_4C_5$(22)+ $^{\nu}C_4C_7$(74) |
| 1299 | 1271 | 1273 | 16 | 6 | $^{\nu}C_3C_5$(36)+$^{\nu}C_4C_5$(32)+ $^{\nu}C_4C_7$(83) |
| 1232 | 1236 | 1261 | 19 | 10 | $^{\nu}C_3C_5$(54)+$^{\nu}C_4C_5$(98)+ $^{\nu}C_4C_7$(37) |
| 1208m | - | 1208 | 7 | 4 | $^{\nu}C_3C_5$(37)+$^{\nu}C_4C_5$(37)+ $^{\nu}C_4C_7$(37) |

| | | | | | |
|---|---|---|---|---|---|
| 1139 | 1129 | 1155 | 9 | 12 | $^{v}C_3C_6(10)$ |
| 1039 | - | 1044 | 1 | 4 | $^{v}O_1C_7(12)$ |
| 946 | 943 | 986 | 0 | 28 | $^{v}C_{10}C_4(52)$ |
| 929 | 931 | 922 | 2 | 23 | $^{v}C_3C_9(16)$ |
| 895 | 893 | 898 | 6 | 66 | $^{\beta}C_5C_4C_3(21)$ |
| 872 | - | 875 | 0 | 4 | $^{\beta}C_5C_3C_6(59)$ |
| 801 | 818 | 819 | 1 | 1 | $^{\beta}H_{18}O_1C_7(15)$ |
| 784 | 784 | 779 | 0 | 0 | $^{\beta}H_{11}C_5C_3(45)+^{\beta}H_{12}C_6C_8(37)+^{\beta}H_{13}C_8C_7(16)$ |
| 769 | 769s | 769 | 52 | 14 | $^{\beta}H_{11}C_5C_3(35)+^{\beta}H_{12}C_6C_8(77)+^{\beta}H_{13}C_8C_7(26)$ |
| 741s | - | 743 | 8 | 2 | $^{\beta}H_{11}C_5C_3(39)+^{\beta}H_{12}C_6C_8(38)+^{\tau}H_{11}C_5C_3C_6(62)$ |
| 732 | 719 | 737 | 5 | 6 | $^{\beta}H_{14}C_9H_{16}(17)+^{\beta}H_{15}C_9H_{14}(75)+^{\beta}H_{15}C_9H_{16}(85)$ |
| 668 | 672 | 691 | 3 | 9 | $^{\beta}H_{14}C_9H_{16}(95)+^{\beta}H_{15}C_9H_{14}(15)+^{\beta}H_{15}C_9H_{16}(25)$ |
| 647 | 636 | 691 | 3 | 9 | $^{\beta}H_{14}C_9H_{16}(65)+^{\beta}H_{15}C_9H_{14}(51)+^{\beta}H_{15}C_9H_{16}(58)$ |
| 620 | | 614 | | | $^{\tau}H_{12}C_6C_3C_9(32)+ {}^{\tau}H_{13}C_8C_7C_4(12)$ |
| 603 | - | 593 | 2 | 28 | $^{\tau}H_{11}C_5C_3C_6(26)+^{\tau}H_{12}C_6C_3C_9(13)+ {}^{\tau}H_{13}C_8C_7C_4(24)$ |
| 547s | - | 561 | 1 | 10 | $^{\tau}H_{11}C_5C_3C_6(42)+^{\tau}H_{15}C_3C_5C_9(51)+ {}^{\tau}H_{16}C_3C_5C_9(49)$ |
| 539 | 530 | 518 | 27 | 16 | $^{\tau}H_{11}C_5C_3C_6(79)$ |
| 480m | 479 | 496 | 8 | 8 | $^{\beta}H_{17}C_{10}O_2(15)+ {}^{\tau}H_{11}C_5C_3C_6(62)$ |
| 460 | 454 | 462 | 3 | 5 | $^{\beta}O_2C_4C_{10}(15)$ |
| - | 434 | 436 | 8 | 6 | $^{\beta}C_5C_4C_3(15)+^{\beta}C_5C_6C_3(15)+^{\beta}C_7C_8C_6(37)$ |
| - | 350 | 381 | 1 | 0 | $^{\beta}C_5C_4C_3(15)+^{\beta}C_5C_6C_3(15)+^{\beta}C_7C_8C_6(15)$ |
| - | 326 | 342 | 3 | 0 | $^{\beta}C_5C_4C_3(67)+^{\beta}C_5C_6C_3(15)+^{\beta}C_7C_8C_6(39)$ |

| | | | | | |
|---|---|---|---|---|---|
| - | 247 | 239 | 2 | 2 | $^{\beta}O_1C_7C_8(74)+ {}^{\tau}H_{11}C_5C_4C_7(72)$ |
| - | 153 | 132 | 0 | 3 | $^{\beta}C_{10}C_7C_4(15)+ {}^{\tau}H_{11}C_5C_4C_7(62)$ |
| - | 124 | 113 | 9 | 5 | $^{\tau}H_{10}C_2C_1C_6(48)+ {}^{\tau}H_{13}C_8C_7C_4(34)$ |
| - | 119 | 109 | 1 | 2 | $^{\tau}H_{11}C_5C_3C_6(46)+ {}^{\tau}H_{13}C_8C_7C_4(34)$ |
| | 102 | 98 | 8 | 0 | $^{\beta}C_9C_6C_3(15)+ {}^{\tau}H_{13}C_8C_7C_4(34)$ |
| | 93 | 91 | 2 | 1 | $^{\tau}H_{18}O_1C_4C_7(62)$ |
| | 89 | 85 | 14 | 8 | $^{\tau}H_{11}C_5C_3C_6(62)+ {}^{\tau}H_{13}C_8C_7C_4(34)$ |
| | 84 | 80 | 5 | 6 | $^{\tau}H_{11}C_5C_3C_6(28)+{}^{\tau}H_{12}C_6C_3C_9(30)$ + $^{\tau}H_{13}C_8C_7C_4(34)$ |
| | 78 | 77 | 7 | 3 | $^{\tau}H_{11}C_5C_3C_6(50)+{}^{\tau}H_{12}C_6C_3C_9(72)$ + $^{\tau}H_{13}C_8C_7C_4(55)$ |
| | 73 | 71 | 1 | 2 | $^{\tau}H_{11}C_5C_3C_6(60)+{}^{\tau}H_{12}C_6C_3C_9(62)$ + $^{\tau}H_{13}C_8C_7C_4(66)$ |
| | 69 | 67 | 16 | 13 | $^{\tau}H_{11}C_5C_3C_6(31)+{}^{\tau}H_{15}C_3C_5C_9(60)$ + $^{\tau}H_{16}C_3C_5C_9(74)$ |
| | 59 | 56 | 7 | 4 | $^{\tau}H_{11}C_5C_3C_6(56)+{}^{\tau}H_{15}C_3C_5C_9(70)$ + $^{\tau}H_{16}C_3C_5C_9(63)$ |
| | 58 | 57 | 3 | 0 | $^{\tau}H_{11}C_5C_3C_6(43)+{}^{\tau}H_{15}C_3C_5C_9(70)$ + $^{\tau}H_{16}C_3C_5C_9(52)$ |

ν:Stretching; sym: symmetric stretching; β: inplane bending; γ: out of plane bending; asym: asymmetric; τ:torsion ; s: strong; vs: verystrong; m:medium; w:weak; vw: very weak.

### 4.2.2 Ring vibrations

The ring carbon–carbon stretching vibrations occur in the region 1430–1625 $cm^{-1}$ [12]. The theoretically computed value of the HMP molecule is identified at 1644$cm^{-1}$. The C-C aromatic stretch, known as semicircle stretching, predicted at 1590 $cm^{-1}$. The in-plane deformation vibration is at higher frequencies than the out-of-plane vibrations. The theoretically computed value is 721 $cm^{-1}$. Usually the bands around 2900–3100 $cm^{-1}$ are assigned to C-H stretching vibration in aromatic compound. They are not appreciably affected by the nature of the substituents. The C-H stretching vibration is assigned to 3041, 3019, 2978$cm^{-1}$ in FT-IR spectrum, which is observed in the calculated spectrum at 3048, 3015 and 2999 $cm^{-1}$.

### 4.3. Natural bond orbital analysis

NBO analysis is a dominant method to analyse the intra- and inter-molecular charge transfer interactions, hydrogen bonding, conjugation-hyperconjugation- interactions. The charge delocalization due to the interactions between filled and antibonding orbitals can be analysed through NBO method. NBO analysis has been performed on the molecule at the MP2/6-31G (d) level in order to elucidate the conjugation, hyperconjugation and delocalization of electron density within the molecule

In title compound the stabilization energy contributions from the σ ($C_3$-$C_5$) → σ*($C_4$-$C_{10}$) interaction is 12.175 kJ/mol and σ ($C_4$-$C_7$) → σ*($C_7$-$C_8$) interaction is 20.823kJ/mol. The highest stabilization energy

contributions occurred due to OH group and hydroxy methyl group and $CH_2$-OH groups are attached in ring C atom. The σ ($C_6$-$C_8$) → σ*($O_1$-$C_7$) interaction is 17.656 kJ/mol and σ ($C_7$-$C_8$) → σ*($C_4$-$C_7$) interaction is 19.874 kJ/mol.

**Table: 3 Second order perturbation theory of fock matrix in NBO basis.**

| Donor NBO(i) | E.D/e | Acceptor NBO(j) | E.D/e | $E^{(2)}$/kJmol$^{-1}$ |
|---|---|---|---|---|
| σ($C_3$-$C_5$) | 1.975<br>-0.702 | σ*($C_4$-$C_{10}$) | 0.047<br>0.455 | 12.175 |
| σ($C_4$-$C_5$) | 1.972<br>-0.705 | σ*($O_1$-$C_7$) | 0.023<br>0.317 | 13.012 |
| σ($C_4$-$C_7$) | 1.966<br>-0.706 | σ*($C_7$-$C_8$) | 0.024<br>0.563 | 20.823 |
| σ($C_4$-$C_{10}$) | 1.979<br>-0.685 | σ*($C_7$-$C_8$) | 0.024<br>0.563 | 11.422 |
| σ($C_6$-$C_8$) | 1.968<br>-0.699 | σ*($O_1$-$C_7$) | 0.023<br>0.317 | 17.656 |
| σ($C_7$-$C_8$) | 1.976<br>-0.725 | σ*($C_4$-$C_7$) | 0.031<br>0.529 | 19.874 |

$E^{(2)}$ is the energy of hyperconjugative interactions.

**TABLE: 4 possible hyper conjugation interaction of HMP molecule**

| Donor NBO(i) | E.D/e | Acceptor NBO(j) | E.D/e | $E^{(2)}$/ KJ mol$^{-1}$ | H.O |
|---|---|---|---|---|---|
| $O_1$ | 1.979<br>-0.604 | σ*($C_4$-$C_7$) | 0.412<br>0.039 | 25.89 | $Sp^2$ |
| $O_2$ | 1.982<br>-0.626 | σ*($C_4$-$C_{10}$) | 0.028<br>0.409 | 19.51 | $Sp^2$ |

### 4.4. Mulliken atomic charge analysis

Charge analysis has an important role in molecular system because it gives reliable characterization of the charge distribution in a molecular system. Atomic charges of molecules influence the chemical stability, polarizability, dipole moment etc. The two methods predicted same properties but the natural population analysis (NPA) satisfies Pauli's exclusion principle and resolves the basis set dependence problem of Mulliken's charge analysis. Atomic charges of individual atom have been computed using MP2/6-31G (d) basis set. The summary of natural population analysis and Mulliken atomic charges are presented in Table.5. The charge distribution plots are depicted in Fig. 3. Natural atomic charges are different from Mulliken atomic charges. Atom, $C_7$ is positive (0.345e) charge which suggests an extensive charge delocalization in the entire molecule through $C_4$-$C_7$. $C_7$ of benzene ring shows more positive than other due to the direct attachment of high electronegative $O_1$ atom of hydroxyl group. The more negative values on $C_9$ atom of $CH_3$ group leads to a redistribution of electron density. All hydrogen atoms shows

positive charge, in which $H_{18}$ (0.458) and $H_{20}$ (0.453) have more positive and these hydrogen atoms are part of $C_8$-$H_{13}$…$O_1$ and $C_5$-$H_{11}$…$O_2$ hyperconjugative interactions.

**Table : 5 Mulliken and natural atomic charges of HMP molecule**

| Atom | Mulliken atomic charges | Natural charges(e) |
|---|---|---|
| $O_1$ | -0.366 | -0.678 |
| $O_2$ | -0.356 | -0.668 |
| $C_3$ | -0.086 | -0.231 |
| $C_4$ | -0.169 | -0.131 |
| $C_5$ | -0.033 | -0.174 |
| $C_6$ | -0.092 | -0.002 |
| $C_7$ | 0.137 | 0.345 |
| $C_8$ | -0.065 | -0.260 |
| $C_9$ | -0.257 | -0.581 |
| $H_{11}$ | 0.058 | 0.153 |
| $H_{12}$ | 0.078 | 0.197 |
| $H_{13}$ | 0.090 | 0.211 |
| $H_{14}$ | 0.110 | 0.201 |
| $H_{15}$ | 0.111 | 0.201 |
| $H_{16}$ | 0.125 | 0.207 |
| $H_{17}$ | 0.104 | 0.154 |
| $H_{18}$ | 0.239 | 0.458 |
| H19 | 0.104 | 0.154 |
| $H_{20}$ | 0.240 | 0.453 |

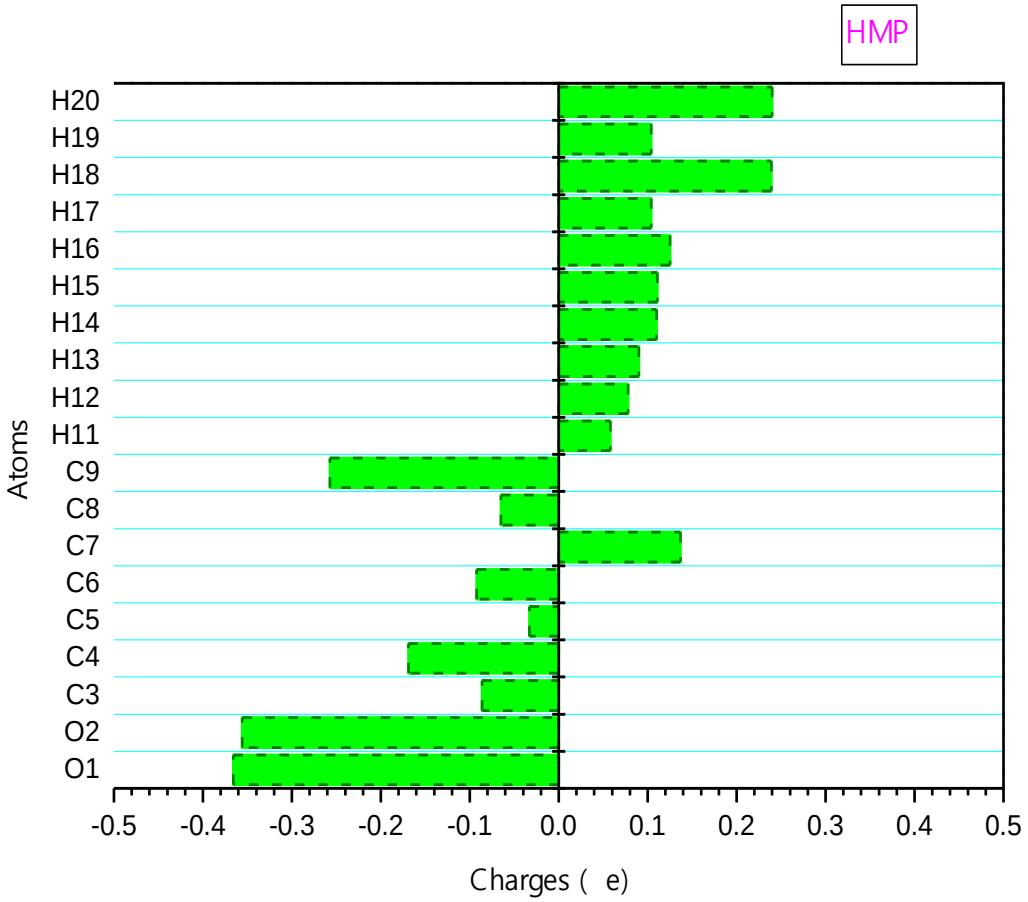


Fig.3 Charge distribution plot of the HMP molecule

**4.5 UV-visible spectral analysis**

UV-visible spectra were taken in acetone solvent. UV-Visible spectra shows three intense transitions in acetone environment is strong absorption band at 318nm (H→L), which corresponds to n→π* transition by a number of transition with C.I expansion coefficients 0.0001 and the oscillate strength 0.66521. And the other two bands are due to π →π* transitions (291nm) and π →σ* transitions (234nm). Electronic transitions are usually classified according to the orbitals engaged or to specific part of the molecule involved. Common types of electronic transitions in organic compounds are π (donor) π*(acceptor) and n→π*. Polarizable continuum models (PCMs) [13] have emerged in the last recent decades as the most effective tools to treat bulk solvent effects for both the ground and excited states. The calculated dipole moment absorption wavelengths (λ), oscillator strengths (f) and excitation energies (E) for various solvents are presented in Table 6. The corresponding calculated values in acetone, water and ethanol in H→L transition feature. In Ethanol (325nm) solvent very high calculated value shows H→L transition. Corresponding excitation energy (3.850 eV) is very low compared with other solvents. In water solvent the high dipole moment is (6.2456D).

**Table: 6 Calculated and experimental electronic absorption spectrum of bona with different solvents at PCM–TD DFT basis set**

| Solvents | Transition feature | Oscillator strength | C.I Expansion Coefficient | Excitation Energy (eV) | Calculated Wavelength (nm) | Experimental Wavelength (nm) | Dipole Moment (D) | Assign ments |
|---|---|---|---|---|---|---|---|---|
| Acetone | H→L | 0.66521 | 0.0001 | 3.888 | 321.82 | 318 | 6.1557 | n→π* |
| | H+1→L+1 | -0.147 | 0.1255 | 4.266 | 292.58 | 291 | | π →π* |
| | H→L+1 | 0.658 | 0.193 | 5.255 | 232.91 | 234 | | π →σ* |
| Water | H→L | 0.6655 | 0.0001 | 3.897 | 318.10 | | 6.2456 | π →π* |
| | H+1→L+1 | -0.147 | 0.1237 | 4.260 | 291.12 | | | n→π* |
| | H→L+1 | 0.658 | 0.192 | 5.254 | 235.67 | | | π →σ* |
| Ethanol | H→L | 0.66529 | 0.0001 | 3.850 | 325.46 | | 6.1766 | n→π* |
| | H+1→L+1 | -0.1473 | 0.1256 | 4.264 | 290.73 | | | π →π* |
| | H→L+1 | 0.6589 | 0.1941 | 5.254 | 235.97 | | | π →σ* |

### 4.6. NMR spectral analysis

The chemical shift for $C_{13}$ is measured in the range 196.1 to 28.64ppm. The higher chemical shift at $C_3$ is due to the presence of OH group. The decrease in chemical shift at $C_3$ and $C_4$ are due to the substitution of methyl and hydroxyl methyl groups respectively. The calculated value shows close agreement with the experimental data. In proton NMR the values ranges from 10.7 to 2.2ppm. All the methyl hydrogen having chemical shift approximately same (2.2)ppm due to hydroxyl methyl group the chemical shift is increased to 10.7ppm.

### 4.7 Molecular Electrostatic Potential

The molecular electrostatic potential (MESP) mapping is very useful in the investigation of the molecular structure with its physiochemical property relationship [14-16]. The molecular electrostatic potential surface (MESP) displays molecular shape, size and electrostatic potential values and it has been plotted. The MESP map visibly suggest that the region around carbon atoms are linked through oxygen atoms $O_1$ and $O_2$ in hydroxyl and hydroxyl methyl group which represent the most negative potential region (red). The hydrogen atoms attached to the ring show the maximum positive charge (blue). In the colour scheme for the MESP surface red colour indicates electron rich with partially negative charge, blue colour denote slightly electron deficient and partially positive charge, light blue show slightly electron deficient region, yellow colour found to be slightly electron rich region and green colour represent the region of zero potential respectively. The MESP total density clearly shows the presence of more electron density around the carbonyl group characterized by red colour. The predominance of green region in the MESP surfaces corresponds to a potential halfway between the two extremes red and dark blue colour. The MESP and total

density plots for most negative potential (-7.256eV) and most positive potential (7.256eV) by MP2/6-31G (d) method is given in Fig.4.

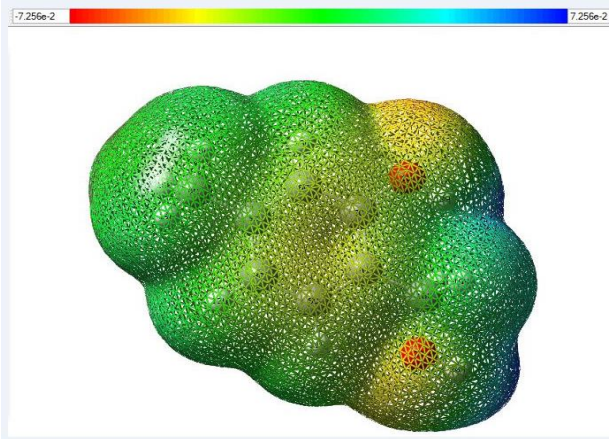


Fig.4. Molecular electrostatic potential of HMP molecule

### 4.8 HOMO-LUMO Energy

Highest occupied molecular orbital (HOMO) and lowest unoccupied molecular orbital (LUMO) are very important parameters for quantum chemistry. HOMO, which can be thought the outermost orbital containing electrons, tends to give these electrons such as an electron donor. On the other hand; LUMO can be thought the innermost orbital containing vacancies to accept electrons [17]. Owing to the interaction between HOMO and LUMO orbital of a structure, transition state, transition of π–π* type is observed with regard to the molecular orbital theory [18]. Therefore, while the energy of the HOMO is directly related to the ionization potential, LUMO energy is directly related to the electron affinity. Energy difference between HOMO and LUMO orbital is called as energy gap, that is an important stability for structures. In addition, plots of (HOMOs) and (LUMOs) are shown in Fig.5. Theoretically, the first hyperpolaizability of the title compound is 1.0019 $x10^{-30}$ times magnitude of urea with greater dipole moment and hyperpolaizability value than urea which shows that the molecule has large NLO optical property. HOMO–LUMO energy gap value is -0.20172eV. The Zero point vibrational Energy, Dipole moment(D), SCF Energy and HOMO-LUMO energy of the HMP molecule are listed in table 7. HOMO – LUMOgap shows that there is energy transfer from hydroxy methyl group to methyl group.

**Table: 7 Zero point vibrational energy, dipole moment (D), SCF energy and HOMO-LUMO energy of the HMP molecule.**

| Zero point vibrational Energy ($KJmol^{-1}$) | Dipole moment(D) | SCF Energy ($KJmol^{-1}$) | First-order Hyper polarizability ($x10^{-30}$) | HOMO-LOMO eV |
|---|---|---|---|---|
| 434.307 | 2.1502 | -1203710.36 | 1.0019 | -2.66786 |

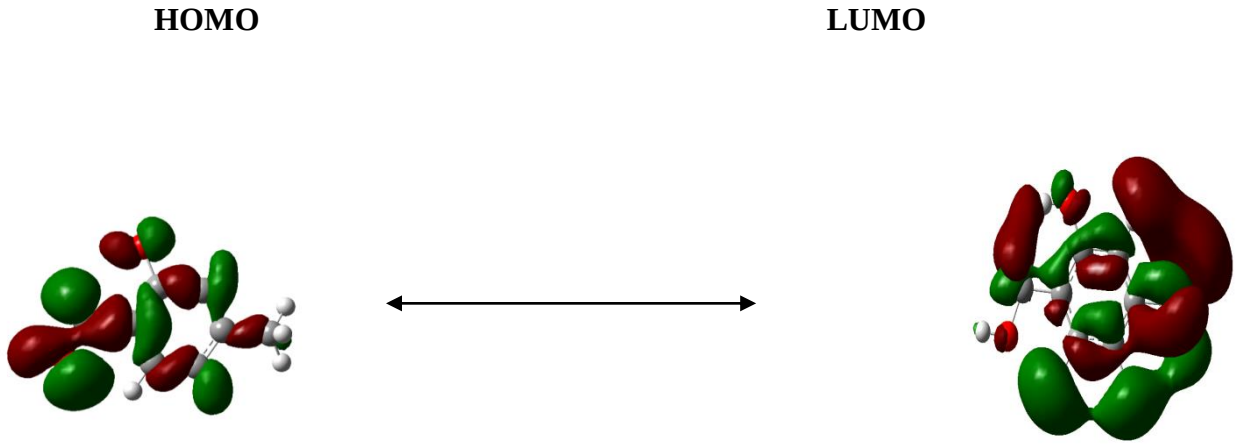


(ΔE=-2.66786eV)

Fig.5: Atomic orbital composition of the molecular orbitals and the electronic transition for HMP molecule

## 5. Powder second harmonic generation (SHG) Test

The SHG efficiency of the title compound is measured by using the Kurtz- Perry powder technique and compared with urea. The sample is subjected to a Q-switched Nd: YAG laser emitting 1064 nm 10 ns pulse width and 5 mJ power. The generated SHG signal at 532 nm is split from the fundamental frequency using an IR separator. A detector connected to a power meter is used to detect SHG and read the energy input and output. The SHG efficiency is compared with urea. An intense green light has been observed and this confirms that the HMP molecule is SHG active. The light observed is highly intense than other samples urea and KDP crystals. This confirms the system has more SHG efficiency when compared to mentioned sample.

### 5.1 Non-Linear Optical (NLO) Properties

The values of the polarizabilities(α) and first hyperpolarizability(β) of the GAUSSION '09 W output are reported in atomic units (a.u) the calculated values have been converted into electrostatic units (esu). In our present study, the total static dipole moment, polarizability and the first hyperpolarizabilitiesof the compound were calculated. Table 4 shows the values of the electric dipole moment (Debye) and dipole moment components, polarizabilities and hyper polarizabilities values. Urea is one of the prototypical molecules and the values of its NLO properties are used frequently as a threshold for comparative purposes. The value of hyperpolarizability of the HMP molecule is about 4.6807 times greater than urea, thus illustrating its potential for the application as NLO material. Although an accurate determination of electronic and vibrational contributions to (hyper) polarizabilities of molecules in the gas phase is interesting in its own right, computational modeling of nonlinear vibrational hyper polarizabilities is still a challenging task.

### 5.2 Potential energy surfaec scan (PES) study

In order to investigate the possible conformations of title compound , potential energy scans were performed for the dihedral angles D($C_8$-$C_7$-$O_1$-$H_{18}$), D($C_5$-$C_3$-$C_6$-$C_9$), at the MP2/6-31G(d) level of theory. The scans were obtained by minimizing the potential energy in all geometrical parameters by varying the

torsion angles at a step of 10◦ in the range of 0-360◦ rotation around the bond. For this rotation potential energy curve has been shown in Fig.6. The geometry is confined to its local minimum as a consequence of imposing symmetry constraints while optimizing geometry. The OH rotation of the torsion angle is D ($C_8$-$C_7$-$O_1$-$H_{18}$) and $CH_3$ rotation for D ($C_5$-$C_3$-$C_6$-$C_9$) angle. The steric effect arising due to weak vander Waals repulsive interaction arises between the positively charge (OH) hydrogen and hydroxy methyl group hydrogen atoms clearly demonstrates that corresponds to the global minimum energy -1211505.4KJ/mol. The OH rotation is maximum obtained at 90º and 270º corresponds to the global maximum energy -1211489.7KJ/mol. $H_{13}$-$H_{18}$ distance occured in (3.4753Å) at an angle 180º, due to the steric interaction. In HMP molecule, the bond $H_{13}$-$H_{18}$ distance minimum occured in 2.2780 at an angle 0º and maximum distance occured in (2.9321Å) at an angle 90º. In $CH_3$ rotation the maximum angle around 0º, 120º, 240 º and 360 º.

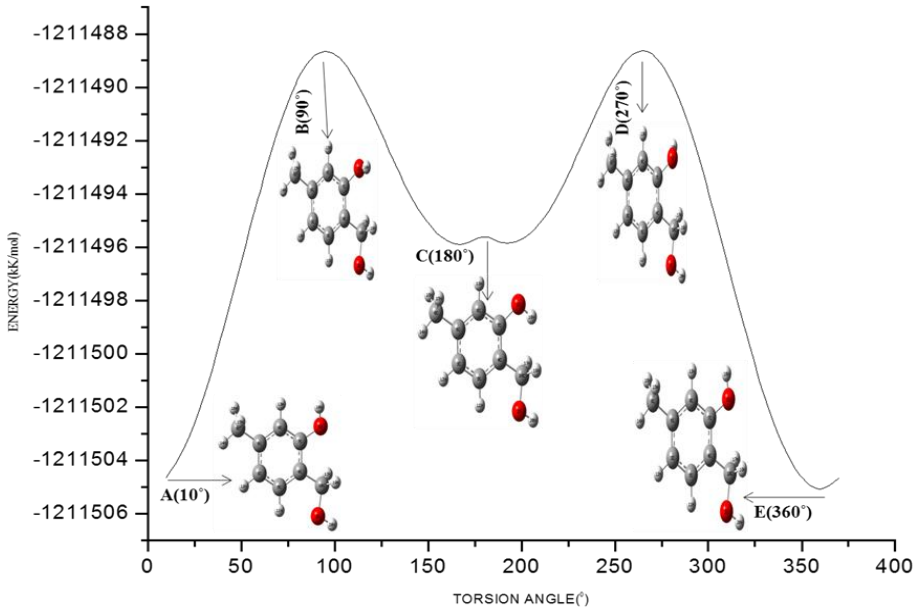


Fig.6: Potential energy surface scan of HMP molecule for oh rotation about dihedral angles D ($C_8$-$C_7$-$O_1$-$H_{18}$)

**Table: 8 Detailed potential energy surface scan study of HMP molecule**

| Angle (º) | Energy ($kJmol^{-1}$) | Distance (A°) | | | | | |
|---|---|---|---|---|---|---|---|
| | | $O_1$...$C_7$ | $O_1$...$C_{19}$ | $O_1$...$H_{18}$ | $H_{13}$...$H_{18}$ | $H_{18}$...$H_{19}$ | $H_{17}$...$H_{18}$ |
| 0 | -1211505.469 | 1.3737 | 2.6772 | 0.9624 | 2.2870 | 3.5506 | 3.6507 |
| 90 | -1211489.716 | 1.3941 | 2.7481 | 0.9629 | 2.9321 | 2.7349 | 3.2855 |
| 180 | -1211494.967 | 1.3741 | 2.7797 | 0.9608 | 3.4753 | 2.1207 | 2.3332 |
| 270 | -1211489.716 | 1.3941 | 2.7658 | 0.9629 | 2.9323 | 3.2818 | 2.7329 |
| 360 | -1211505.469 | 1.3730 | 2.6875 | 0.9625 | 2.2763 | 3.6041 | 3.6101 |

### 5.3 Thermodynamic Properties

The variation in Zero-Point Vibrational Energies (ZPVEs) seems to be significant. On the basis of vibrational analysis and statistical thermodynamics, the standard thermodynamic functions heat capacity (C) entropy (S) and enthalpy changes (ΔH) for the HMP molecule where calculated using THERMO.PL [19] and are listed in Table 8. As observed from table, the values of Cv, S and ΔH all increases with increase of temperature which is attributed to the enhancement of the molecular vibration as the temperature increases. The correlation graphics of those parameters are shown in Fig.7 up to the temperature range of 100K to 1000K. Thermal energy gradually increases with temperature. The calculated results reveal the following thermodynamic parameters. The calculated SCF energy, ZPVE and dipole moment values are -1203710.36kJmol$^{-1}$, 434.307kJ/mol and 2.1502D.

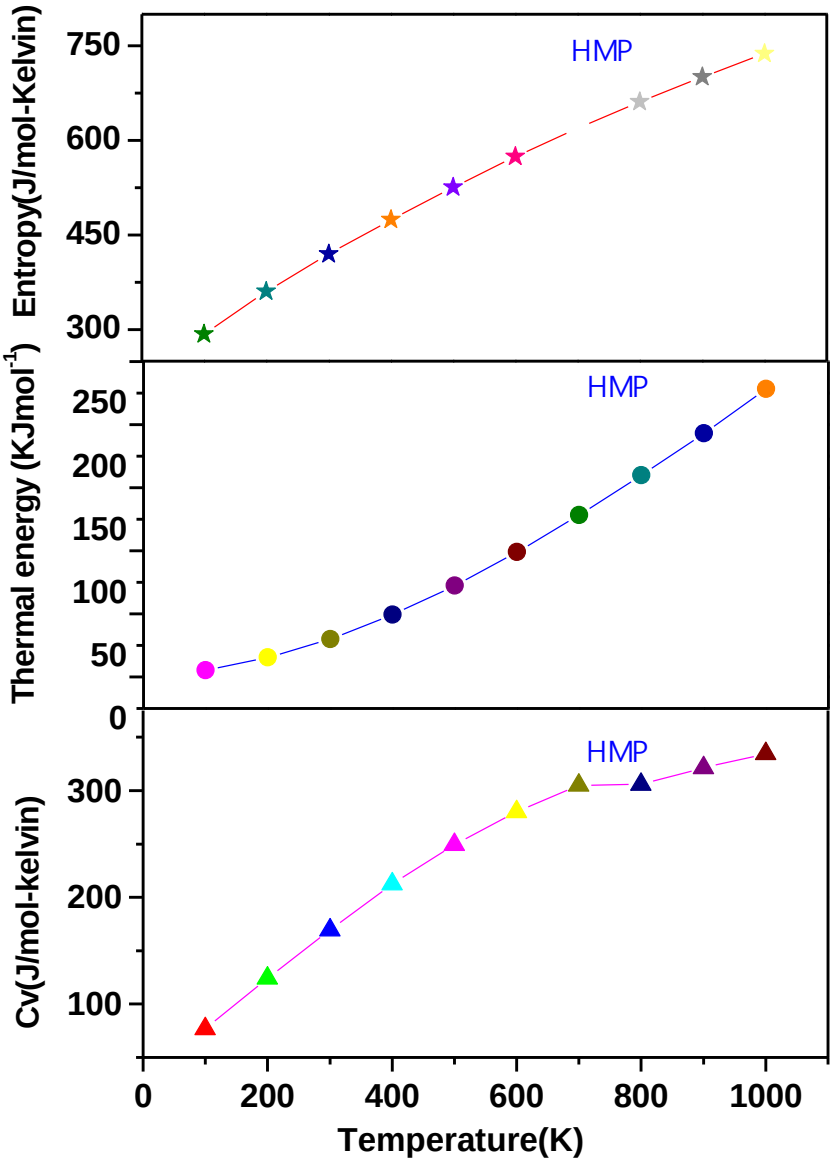


Fig.7. Thermodynamic functions plot of HMP molecule

**Table: 9 Calculated thermodynamic functions values of HMP molecule**

| Temperature(K) | Specific heat capacity Cv (J/mol-kelvin) | Thermal energy ($KJmol^{-1}$) | Entropy(J/mol -Kelvin) |
|---|---|---|---|
| 100 | 76.8 | 5.3 | 292.6 |
| 200 | 124.1 | 15.4 | 360.7 |
| 300 | 169.3 | 30.0 | 419.6 |
| 400 | 212.3 | 49.2 | 474.3 |
| 500 | 249.3 | 72.3 | 525.8 |
| 600 | 279.9 | 98.8 | 574.1 |
| 700 | 305.1 | 128.1 | 619.2 |
| 800 | 305.8 | 159.7 | 661.3 |
| 900 | 321.4 | 193.2 | 700.8 |
| 1000 | 334.5 | 228.3 | 737.8 |

## 6. Conclusions

In the present work the complete molecular structural analysis and vibrational frequencies of the fundamental modes of title compound has been determined using MP2 calculations using 6-31G (d) basis is set. The detailed interpretation of the normal modes has been made on the basis of PED calculations. The computed optimized parameters are in good agreement with those obtained by experimental data. $C_4$-$C_{10}$ bond length is decreased while comparing to $C_3$-$C_9$. This decreasing bond length is due to the presence of hydroxyl methyl group. The Mulliken atomic charge analysis shows that the atom $C_7$ is more positive due to extended conjugation and hydroxyl methyl group. The NBO analysis shows that the highest energy contributions occured in the OH group and hydroxy methyl groups are attached in ring C atom. It is supported by the low value of electron density. In UV-visible spectral analysis the intense absorption position is observed at 318nm which corresponds to n→л* transition. The low value of HOMO-LUMO energy gap shows the NLO active nature of the title compound. The first order hyperpolarizability shows the nonlinear optical activity. The calculated SCF energy, zero point vibrational energy and dipole moment also shows the NLO activity. The correlations between the temperature and statistical thermodynamical parameters are also obtained. It was seen that the specific heat capacity, entropy and enthalpy are gradually increased with the increasing temperature owing to the intensities of the molecular vibrations increases with increasing temperature.

**References**

[1] DS Chemla, Zyss J. Nonlinear optical properties of organic molecules and crystals. Orlando: Academic Press; 1987.

[2] G.W.T.M.J. Frisch, H.B. Schlegel, G.E. Scuseria, M.A. Robb, J.R. Cheeseman, G. Scalmani, V. Barone, B. Mennucci, G.A. Petersson, H. Nakatsuji, M. Caricato, X. Li, H.P. Hratchian, A.F. Izmaylov, J. Bloino, G. Zheng, J.L. Sonnenberg, M. Hada, M. Ehara, K. Toyota, R. Fukuda, J. Hasegawa, M. Ishida, T. Nakajima, Y. Honda, O. Kitao, H. Nakai, T. Vreven, J.A. Montgomery Jr., J.E. Peralta, F. Ogliaro, M. Bearpark, J.J. Heyd, E. Brothers, K.N. Kudin, V.N. Staroverov, R. Kobayashi, J. Norm, K. Raghavachari, A. Rendell, J.C. Burant, S.S. Iyengar, J. Tomasi, M. Cossi, N. Rega, J.M. Millam, M. Klene, J.E. Knox, J.B. Cross, V. Bakken, C. Adamo, J. Jaramillo, R. Gomperts, R.E. Stratmann, O. Yazyev, A.J. Austin, R. Cammi, C. Pomelli, J.W. Ochterski, R.L. Martin, K. Morokuma, V.G. Zakrzewski, G.A. Voth, P. Salvador, J.J. Dannenberg, S. Dapprich, A.D. Daniels, O. Farkas, J.B. Foresman, J. V. Ortiz, J. Cioslowski, D.J. Fox, Wallingfort CT, Edition 2009.

[3] G.A. Zhurko, D.A. Zhurko, Chemcraft, Available from http://www.chemcraftprog.com, 2005.

[4] Dennigton II R., Keith, T. Millam, J. GaussView, Version 4.1.2, Semichem, Inc., 2007. Shawnee Mission, KS.

[5] Jamroz, M.H. Vibrational Energy Distribution Analysis: VEDA 4 Program, Warsaw, 2004.

[6] Reed, A.E. Curtiss, L.A. Weinhold, F. Chem. Rev. 88 (1988) 899.

[7] Onida, Reining, G. L. Rubio, A. Rev. Mod. Phys. 74 (2002) 601.

[8] Acta Cryst. (2006). E62, o282-o283 https://doi.org/10.1107/S1600536805041887

[9] A. Ramoji, J. Yenagi, J. Tonannavar, Spectrochim. Acta 69A (2008) 926.

[10] G. Socrates, Infrared Characteristic Group Frequencies, John Wiley, GB, 1980.

[11] G. Varsanyi, Vibrational Spectra of Benzene Derivatives, Akademiai Kiado, Budapest, 1969.

[12] F.R. Dollish, W.G. Fateley, F.F. Bantley, Characteristic Raman Frequencies of Organic Compounds, Wiley, New York, 1974. 170.

[13]. J.Tomasi, B. Mennucci, R. Cammi, Chem. Rev. 105 , 2999. (2005)

[14] Politzer, P. Truhlar (Eds.), D.G. Chemical Application of Atomic and Molecular Electrostatic Potentials, Plenum, New York, 1981.

[15] Politzer, P. Daiker, K.C. The Force Concept in Chemistry, Van Nostrand Reinhold Co., 1981.

[16] Politzer, P. Laurence, P.R. Jayasuriya, K. McKinney, J. Health Perspect. 61 (1985)191.

[17] G. Gece, Corros. Sci. 50, (2008). 2981.

[18] K. Fukui, Theory of Orientation and Stereo Selection, Springer–Verlag, Berlin,

[19] J.S.Murray, K.Sen, Molecular Electrostatic Potentials, Concepts and Applications, Elsevier, Amsterdam, 1996.